RESEARCH ARTICLE | AUGUST 16 2022

Post-field ionization of Si clusters in atom probe tomography: A joint theoretical and experimental study ⊘

Ramya Cuduvally ✉; Richard J. H. Morris; Giel Oosterbos; ... et. al

Check for updates

CrossMark

View Online   Export Citation

Articles You May Be Interested In

Sustainability in PFI project: Concept and perception of the stakeholders

AIP Conference Proceedings (October 2018)

A review on the need to integrate sustainability elements for PFI's project in Malaysia

AIP Conference Proceedings (October 2018)

Weissella paramesenteroides from intestine of Indonesian eel (Anguilla bicolor McClelland) and their potential antimicrobial property

AIP Conference Proceedings (October 2018)

AIP Publishing

Post-field ionization of Si clusters in atom probe tomography: A joint theoretical and experimental study

View Online · Export Citation · CrossMark

Ramya Cuduvally,[1,2,a),b)] [iD] Richard J. H. Morris,[2] Giel Oosterbos,[1] Piero Ferrari,[1] Claudia Fleischmann,[1,2]
Richard G. Forbes,[3] [iD] and Wilfried Vandervorst[1,2]

AFFILIATIONS

[1]Quantum Solid-State Physics, KU Leuven, Celestijnenlaan 200D, 3001 Leuven, Belgium
[2]IMEC, Kapeldreef 75, 3001 Leuven, Belgium
[3]Advanced Technology Institute and Department of Electrical and Electronic Engineering, University of Surrey, Guildford, Surrey GU2 7XH, United Kingdom

[a)]Author to whom correspondence should be addressed: cuduvalr@mcmaster.ca
[b)]Present address: Canadian Centre for Electron Microscopy, McMaster University, 1280 Main St West, Hamilton, Ontario L8S 4M1, Canada.

ABSTRACT

A major challenge for atom probe tomography (APT) quantification is the inability to decouple ions that possess the same mass–charge (m/n) ratio but a different mass. For example, $^{75}As^+$ and $^{75}As_2^{2+}$ at ~75 Da or $^{14}N^+$ and $^{28}Si^{2+}$ at ~14 Da cannot be differentiated without the additional knowledge of their kinetic energy or a significant improvement of the mass resolving power. Such mass peak overlaps lead to ambiguities in peak assignment, resulting in compositional uncertainty and an incorrect labeling of the atoms in a reconstructed volume. In the absence of a practical technology for measuring the kinetic energy of the field-evaporated ions, we propose and then explore the applicability of a post-experimental analytical approach to resolve this problem based on the fundamental process that governs the production of multiply charged molecular ions/clusters in APT, i.e., post-field ionization (PFI). The ability to predict the PFI behavior of molecular ions as a function of operating conditions could offer the first step toward resolving peak overlap and minimizing compositional uncertainty. We explore this possibility by comparing the field dependence of the charge-state-ratio for Si clusters (Si_2, Si_3, and Si_4) with theoretical predictions using the widely accepted Kingham PFI theory. We then discuss the model parameters that may affect the quality of the fit and the possible ways in which the PFI of molecular ions in APT can be better understood. Finally, we test the transferability of the proposed approach to different material systems and outline ways forward for achieving more reliable results.

Published under an exclusive license by AIP Publishing. https://doi.org/10.1063/5.0106692

I. INTRODUCTION

Atom probe tomography (APT) is an indispensable pathway for the investigation of nanoscale structure–property relationships in various scientific disciplines including metallurgy,[1] electronics,[2–5] geology,[6] and biology.[7] Quantitative compositional information in APT is contained in the mass spectrum, which is constructed from the time-of-flight of the ions and using the law of energy conservation. While several factors may influence the accuracy of the determined composition, the most important factor is the ability to unambiguously assign the correct chemical identity to each peak observed in the mass spectrum based on its mass/charge (m/n) ratio. Therefore, ions that possess a different mass but the same m/n ratio (i.e., overlapping peaks) present a problem for APT quantification and, subsequently, the reconstruction. For example, it is not possible to differentiate between ions such as $^{14}N^+$ and $^{28}Si^{2+}$ at ~14 Da or molecular ions/clusters of the same species, e.g., $^{75}As_2^+$ and $^{75}As_4^{2+}$ at ~150 Da. Such mass peak overlaps will lead to ambiguities in peak assignment and ultimately result in a compositional uncertainty.

For the case of the complete overlap between singly and multiply charged clusters, e.g., $^{75}As_2^+$ and $^{75}As_4^{2+}$ at ~150 Da, potentially,

one could differentiate them discreetly[8] based on their kinetic energy. Although research is currently focused on enabling kinetic energy discrimination for APT,[8,9] no such technology has yet been practically implemented for commercial instruments since they are still in their initial stage of development. In some cases where the overlapping species has more than one stable isotope, it may be possible to use isotope-constrained methods[10] to (collectively[8]) discriminate them. However, such techniques are essentially inapplicable to monoisotopic species such as As and P that are important elements in many nano-electronic devices for which APT is extensively used in fabrication process development and control. With the advent of III-V electronics, a plethora of compound materials including GaAs, InGaAs, InP, and InGaAsP are now found ubiquitously in optoelectronics, photonics, photovoltaics, and high-speed analog/RF devices.[11–14] Furthermore, As and P are commonly used as the n-type dopants in the more conventional Si or SiGe based electronic devices.[15,16] The problems associated with As and P are enhanced further as both these elements have a preferential tendency to field-evaporate as clusters,[17,18] thus increasing the probability for numerous peak overlaps and consequently a huge composition quantification uncertainty.

An alternative solution for improving quantification accuracy would be through accurately predicting the level of peak overlap between cluster ions based on the analysis conditions. In this work, we outline a novel approach to achieve this using the post-field ionization (PFI) theory developed for monoatomic ions by Kingham[19] and adapting for clusters. The cluster ionization energies (IEs), which are unknown, were computed using density functional theory (DFT). Subsequently, the PFI probability for the various charge-states of the clusters was estimated as a function of the electric field. The validity of these predictions was then examined against experimental APT data of Si operating in the laser-assisted mode. Si was chosen because it exhibits extensive clustering (up to Si_7) for certain operating conditions[20] and has three stable isotopes. Hence, the peak overlap between the various Si clusters, e.g., $^{28}Si^+$ and $^{28}Si_2^{2+}$ at ~28 Da and $^{28}Si_2^+$ and $^{28}Si_4^{2+}$ at 56 Da, are resolvable using the conventional isotopic peak deconvolution approach. This enabled a quantitative evaluation of our proposed theoretical approach as a standalone technique for resolving peak overlap. Through this joint theoretical and experimental study, we show that the field dependence of the charge-state of Si cluster ions in APT is qualitatively consistent with the predictions of Kingham's PFI theory. We also discuss the reasons for the rather poor quantitative agreement observed between theory and experiment and further demonstrate how improvements can be made to this model based on physically justifiable arguments. Finally, we will assess the transferability of the proposed approach by applying it to resolve overlaps between As clusters that are observed in the APT InGaAs.[17]

A. Theory

In this section, the theoretical principles governing the PFI model proposed by Kingham[19] will be outlined. We will also highlight some of the criticism that the Kingham model received in the later years and the associated implications. Since not all derivations/assumptions were explicitly stated in Kingham's paper,[19] reproducing the original calculations is non-trivial. A comprehensive description

of the theoretical framework is included in the supplementary material.

The presence of multiply charged species in APT finds its origin in the processes of field evaporation and PFI. The latter is a process by which a field-evaporated ion (that is being accelerated away from the emitter) loses an additional electron by quantum tunneling from the ion into an empty electronic state of the emitter or into free space. An ion can even be ionized multiple times after field evaporation. The PFI probability is determined by (and increases with) the electric field strength at the apex. Furthermore, the material properties (i.e., the ionization energy and surface work function) also influence the electron tunneling rate and subsequently the PFI probability. The first successful PFI investigations were related to the field evaporation of rhodium. In an experimental investigation, Ernst[21] showed that Rh^{2+} was formed by PFI with excellent agreement between a PFI model and experimental Rh data.[19] Later, Ernst and Jentsch[22] showed that the experiments[20] were consistent with a tunneling mechanism as described above. Further work by Haydock and Kingham[23–25] confirmed these theoretical results, with Kingham[19] subsequently carrying out PFI calculations for many metallic ion species. Following this, Kellogg[26] experimentally investigated the PFI behavior for six other elements and found a satisfactory agreement between Kingham's model and four of these elements (details in Sec. I B). Thus, the general validity of PFI through the Kingham model was established. The Kingham model describes the electric field dependence of the charge-state-ratio (CSR), i.e., $X^{i+}/\sum_i X^{i+}$, (i = 1, 2, …), of any given constituent species (X) in an APT experiment. Since there is currently no easy way to measure the electric field at the apex of a specimen, the Kingham model is typically used to estimate the magnitude of the electric field based on the CSR, which is readily extracted from the mass spectrum.

In the Kingham model,[19] a single parameter fit was used to match Rh experimental data from Ernst,[21] in which the field strength values were determined by a calibration method described in Ref. 27 with an absolute error of at least 15%. The fitting parameter used by Kingham was the effective nuclear potential Z that is seen by the tunneling electron. As previously mentioned, the validity of the model was verified for several other monoatomic ions experimentally. On the other hand, the PFI behavior of molecular/cluster ions has received much less attention thus far. As far as the authors are aware, only three studies (Refs. 28–30) have been reported in the literature pertaining to the post-ionization behavior and observed charge-state of cluster ions in APT, and some of these findings will be discussed in Sec. I B. Nevertheless the validity of Kingham's PFI model has not been experimentally examined thus far for any molecule/cluster. Such a theoretical and experimental comparison is important because the knowledge of cluster PFI behavior as a function of apex field offers the first step toward tackling quantification inaccuracies resulting from peak overlap. For example, in the APT analysis of InGaAs, resolving the overlap between As_2^+ and As_4^{2+} (150 Da) using the PFI theory would involve the following steps.

A. Estimate the field strength using the CSR of a monoatomic species in conjunction with its Kingham curve or, alternatively, another field calibration technique.[26,27]

B. Predict the ratio of $As_4^{2+}/(As_4^+ + As_4^{2+})$ at this field using a theoretical PFI model that is applicable to molecules.

C. Based on (B) and from the number of counts in the As_4^+ peak (which is assumed to not suffer from overlap with As_8^{2+}), calculate the amount of As_4^{2+} present in the peak at 150 Da.

D. Subtract the value found in (C) from the total counts measured at 150 Da to determine the number of As_2^+ ions.

The most important requirement for the procedure described above is B, i.e., the availability of a reliable PFI model for clusters. Following the approach used by Gault et al.[29] and as a first approximation, we extended Kingham's model to clusters by simply replacing the physical quantities of the monoatomic ions with their respective molecular equivalents (this primarily concerns the ionization energies). We then tested the applicability/accuracy of this model using experimental data of CSR vs electric field for Si clusters (Si_2–Si_4). Thus, the objectives of this study were fourfold:

(1) To explore the CSR–field relationship for Si clusters (Si_2, Si_3, and Si_4) experimentally and compare this with the predictions of the PFI theory.

(2) To identify the model parameters that may need modification when considering the PFI of clusters and evaluate the impact of varying each of these parameters on the PFI curves.

(3) To establish whether the predictions are accurate enough to be used for resolving peak overlap between clusters of monoisotopic species.

(4) Build an understanding of the PFI of molecules in APT and outline the ways forward for improving the agreement of the molecular PFI model with experimental data.

B. Critical look at the Kingham model—A review of the literature

The biggest challenge encountered in testing the validity/quantitative accuracy of the analytical PFI model lies in the lack of a method to directly measure the electric field at the specimen apex. Therefore, indirect schemes need to be employed to estimate a value for the field, and this can be subject to significant errors. Thus, any PFI model will only be as good as the apex field estimation method used. Kingham's work[19] was followed up with experimental investigations by Kellogg,[26] wherein the author compared the experimental charge-state evolution of Ni, Mo, Rh, W, Re, Ir, and Pt with the predictions of Kingham's PFI model. To determine the field strength, F, in the experiment, Kellogg used the following calibration formula:

$$F = F_0(V/V_0). \quad (1)$$

Here, F_0 is the evaporation field threshold at 0 K, V is the applied voltage, and V_0 is the threshold (DC) voltage for field evaporation at the base temperature (and in the absence of laser illumination). Note that this field determination method was different to that of Ernst for Rh,[21] which was based on a one-time calibration of the voltage as a function of the electric field by Müller and Young,[27] which in turn was based on a corrected version of the original Fowler–Nordheim theory of field-electron emission. The accuracy of the field values determined by Kellogg and Ernst was

no less than 25% and 15%, respectively.[19,26] Although Kellogg observed some deviations from the Kingham model at low field for W, Re, and Ir, in general, the field value at which one charge-state becomes more abundant than the other was found to be in reasonable agreement with that predicted by the model. For Mo and Pt, however, Kellogg found that although the experimental results confirmed the occurrence of PFI, the agreement with Kingham's model was poor. In the same paper, Kellogg also experimentally investigated the PFI of Si. However, the F_0 value used for field calibration was not taken from the literature but adjusted to yield the best fit to the Kingham model. The value chosen was 35 V/nm. Therefore, for Si, only a qualitative agreement with PFI trends could be established.

This qualitative agreement of the PFI behavior of Si with the Kingham model was also confirmed by Kumar et al. in a separate study.[31] However, they used an F_0 value of 27.5 V/nm to obtain the best fit to the Kingham curves. Note that significant variations in F_0 can be a result of surface contaminants[26] and/or local differences in the binding energy between the atom and the surface.[32] In another study Schreiber et al.[28] explored the post-ionization behavior of Fe and O in the APT characterization of Fe_3O_4. However, their objective was to investigate whether PFI was the driving factor for the formation of multiply charged species and if the fraction of multiply charged species increased with field. Interestingly, they found that the Fe CSR value was not exclusively dictated by field strength but also showed a dependence on the laser pulse energy (LPE) used. Conversely, for O, they found that the fraction of O_2 clusters was purely field dependent and thus the ratio $O^+/(O^+ + O_2^+)$ was a more reliable indicator of the field compared to the Fe CSR. Again, no quantitative comparisons were made with the Kingham model. In a different study, Gault et al.[29] extended the Kingham model to N_2 in order to determine how likely the formation of N_2^{2+} was at the typical values of field strength used in their experiments. They did so by replacing the atomic IEs with those of the molecular ion (N_2). More recently, in their quest for a statistically reliable CSR to indicate the field, the same approach was applied to the TiD_2 molecule by Chang et al.[30] As mentioned previously, this is also the method we will use for Si clusters in this work. However, in their calculation of the Kingham curves, the authors ignored the region close to the tip surface (thus rendering the crossing surface/critical distance irrelevant). We believe that it is important to include the region close to the tip surface in computing the electron tunneling probability since this region is expected to contribute significantly to this probability. This, and the lack of a standardized software/script for the computation of these curves, motivated our own calculations of the Kingham curves, and this is described in detail in the supplementary material.

II. WORKFLOW AND METHODS

A. Workflow

1. Experimental

The details of the experimental data acquisition and treatment are listed below:

(1) Acquisition of experimental data from a Si specimen in laser mode, which allows the evaporation/detection of Si clusters in the mass spectrum.

(2) Application of isotopic peak deconvolution to resolve any mass spectrum peak overlaps between Si and Si_2^{2+}, Si_2^+ and Si_4^{2+}, and Si_3^+ and Si_6^{2+}.

(3) Calculation of the CSR of Si clusters, i.e., $Si_2^{n+}/(Si_2^+ + Si_2^{2+})$, $Si_3^{n+}/(Si_3^+ + Si_3^{2+})$, and $Si_4^{n+}/(Si_4^+ + Si_4^{2+})$, where n = 1, 2.

(4) Estimation of the electric field strength for each operating condition using the Si-CSR, i.e., $Si^{n+}/(Si^+ + Si^{2+})$, where n = 1 or 2, in conjunction with the Kingham curve of monoatomic Si.

(5) Generation of the experimental cluster PFI curves, i.e., the variation in CSR of Si clusters (Si_2, Si_3, and Si_4) as a function of field strength.

2. Theoretical

In the framework proposed by Kingham,[19] the PFI probability of an ion depends on its ionization energy, its atomic mass (m), the surface work function (ϕ), and the principal quantum number of the highest occupied orbital of the atom (m_q). To extend Kingham's model to clusters, the following steps/assumptions were employed.

(1) Since experimental/theoretical values of the higher order IEs of Si clusters were unavailable in the literature, the vertical IEs of Si clusters were computed using DFT (details in Secs. II B and III A, the supplementary material, and Ref. 33).

(2) Using the computed values of IE and the equations for the ionization rate constant (R), ion velocity (u), and post-field-ionization probability (P_t) as given in Sec. I in the supplementary material, the PFI curves for the Si clusters were computed.

(3) The computed PFI curves were then compared with experimental curves (obtained in step 5, Sec. II A 1).

(4) Finally, the parameters that could potentially affect how well the model agrees with the experimental data are discussed.

B. Definitions: Adiabatic and vertical ionization energy

The loss of an electron from a molecule may be accompanied by changes in its geometry since the ground state geometrical configuration of the ion typically differs from that of the neutral. Thus, two variants of the IE can be defined: adiabatic ionization energy (AIE) and vertical ionization energy (VIE).[34] The AIE corresponds to the *minimum* energy required to remove an electron from a neutral molecule and is defined as the energy difference between the vibrational ground state of the neutral and the ion. An adiabatic ionization involves a rearrangement of the molecular nuclei, which is a much slower process than any electronic transition. The VIE, in contrast, corresponds to the energy difference between the neutral and the ion without any change in the geometrical configuration of the constituent nuclei. Since the Franck–Condon approximation[34] dictates that a vertical electronic transition is more favorable than an adiabatic transition, for the ionization energies and the PFI curves of the Si clusters reported here, we chose to compute and use the VIEs.

C. Methods

The experimental data were acquired on the Cameca LEAP 5000 XR from Cameca Pre-Sharpened Microtip (PSM) Array

Coupons[35] consisting of Sb doped Si specimens. UV laser pulse energies (LPEs) over the range of 90–165 pJ were used. Three different specimens from two different PSM array coupons were measured, and the base temperature was maintained at 25, 27, or 50 K. For each operating condition, $\sim 1 \times 10^6$ ions were collected and the LPE was varied such that Si clusters (up to Si_4 or Si_5) were visible in the mass spectrum. The operating conditions for the three different specimens (referred to as experiment 1, 2, and 3) are listed below. The objective of these experiments was to estimate the CSR of the Si clusters (Si_2, Si_3, and Si_4) as a function of the operating conditions. Subsequently, by determining the Si-CSR value at each of these operating conditions and using the Si Kingham curve, the value of the electric field was estimated at each operating condition. Thus, experimental PFI curves for the Si clusters could be generated.

Experiment 1:
(a) Constant LPE of 100 pJ and varying detection rate in steps from 0.5% to 3.5%.
(b) Constant field (floating detection rate) and varying LPE in steps from 100 to 140 pJ. The minimum and maximum set point values of detection rate were 0.5% and 17%.

Experiment 2: Constant detection rate of 1% and varying LPE in steps from 105 to 165 pJ.

Experiment 3: Constant detection rate of 0.5% and varying LPE in steps from 110 to 125 pJ.

The atom probe data were subsequently analyzed using the commercially available Cameca IVAS 3.8.4 and/or custom written MATLAB codes. The isotope-constrained peak deconvolution algorithm was applied to the experimental data using the built-in peak decomposition functionality within IVAS prior to calculating the CSRs of Si clusters. DFT calculations were performed with the ORCA 4.1.1 software package[36] to determine the Si cluster ionization energies. The range-separated hybrid ωB97X-D3 exchange–correlation functional,[37] which includes a dispersion correction and the large def2-TZVP basis-set[38] were used. Prior to selecting the functional, several other functionals, namely, PBE, TPSS, B3LYP, and the CAM-B3LYP-D3, were used, in addition to the ωB97X-D3, to compute the first AIE and bond lengths of Si clusters (1–7). These results were then compared with experimental data reported in the literature.[39] The details of these calculations along with the atomic coordinates of the energy optimized Si clusters are given in the supplementary material and previously reported by Oosterbos.[33] It was found that the ωB97X-D3 functional yielded the best match with experiment data and hence was chosen for computation of the higher order VIEs. The spin state corresponding to the most stable geometry for each cluster was determined and used here as previously reported by Oosterbos.[33] Finally, to ensure that the computed geometry and spin of the clusters corresponded to the true minima in the potential energy curve, the second derivative test was applied.

III. RESULTS

A. Theoretical

The VIEs for the Si clusters calculated by DFT are given in Table I. The details of the DFT calculations can be found in the supplementary material and Ref. 33. For comparison, the IEs of

TABLE I. VIEs of Si clusters (Si$_2$–Si$_4$) computed with DFT using the ωB97X-D3 functional and the def2-TZVP basis-set. Si IEs are given in row 1 for comparison with clusters.

Cluster size	First IE (eV)	Second IE (eV)	Third IE (eV)
1	8.15	16.35	33.49
2	7.93	15.82	20.28
3	8.22	14.40	20.18
4	8.29	13.85	19.49

Si[39,40] are also given. The primary interest for this study is the second IE of the clusters, and these values are found to be smaller than the second IE of monoatomic Si (Table I).

The values of VIE determined were used in the computation of the PFI curves for Si clusters, which are shown in Fig. 1. The other parameters, i.e., Z, m_q, and ϕ, used in the calculations were assumed to be identical to those of Si. These parameters will be re-visited in Sec. IV and the supplementary material. For each species, the electric field value corresponding to the (50% CSR) crossover point is indicated by labels 1, 2, 3, and 4, which correspond to 19.6, 18, 14.4, and 13 V/nm, for Si, Si$_2$, Si$_3$, and Si$_4$, respectively. We will refer to this electric field value as the F^{50} value from now on.

B. Experimental

An example of a Si mass spectrum is shown in Fig. 2 and is representative of the mass spectra obtained for all the different operating conditions explored in this study. Although Si clusters up to Si$_5$ were detected, we limit our discussion to Si$_2$, Si$_3$, and Si$_4$ due

FIG. 2. Mass spectrum of Si obtained on the LEAP 5000 XR at an applied LPE of 125 pJ, Si^{2+}/(Si$^+$ + Si^{2+}) = 0.02, base temperature of 25 K, and set point detection rate of 1%.

to insufficient statistics of clusters larger than these. As expected, there were significant peak overlaps in the mass spectra, which were readily resolved using isotopic peak deconvolution. For example, when using an LPE of 100 pJ and a set point detection rate of 1% (experiment 1), the Si$_2^{2+}$-CSR before and after applying the peak deconvolution algorithm were found to be 0.048 and 0.543, respectively. This is a significant deviation that would result in an incorrect conclusion about the accuracy of the theoretical predictions if not taken in account.

To visualize the trend in the experimental data and to account for the known tip asymmetry (and thus local differences in electric field strength), the dataset for each operating condition was divided into two regions, as shown in Fig. 3. The apex electric field strength is expected to be lower on the laser side due to the larger local radius of curvature, which is reflected in the density plot [Fig. 3(a)] and the Si-CSR distribution [Fig. 3(b)].

Using the Si-CSR and Kingham curve, a value of the electric field for each analysis condition was determined. Assuming this electric field value, the corresponding PFI curves for Si$_2$ [Fig. 4(a)], Si$_3$ [Fig. 4(b)], and Si$_4$ [Fig. 4(c)] were constructed. For comparison, the theoretical PFI curves (from Fig. 1) for each cluster size are indicated by the solid lines. The PFI of the Si clusters appear to follow an electric field-dependent trend consistent with the Kingham PFI theory, i.e., the relative abundance of Si$_2^{2+}$ and Si$_3^{2+}$ (blue symbols) clearly increase with electric field. From the experimental data, the electric field value corresponding to F^{50} occurs at ~17.7 V/nm for both Si$_2$ and Si$_3$. Moreover, the Si$_2$ cluster shows a good agreement between the theoretically calculated PFI plot and the experimental data. However, the agreement between theory and experiment is poor for Si$_3$ and Si$_4$. Additionally, for Si$_4$, a crossover point could not be identified from the experimental data alone. One possibility is that we are in an electric field regime greater than F^{50}, where the CSR is not as sensitive to the electric field and where the Si$_4^{2+}$ counts have begun to dominate over Si$_4^+$. If this were the case, the data indicate that the crossover point for Si$_4$ would appear to lie below 17 V/nm [a possible fit to the experimental data is shown in Fig. 5(b)].

Note that for the experimental data, the accuracy of the electric field values (which will effectively correspond to horizontal error bars) is determined by the counting statistics error on the Si-CSR, which when translated to electric field was found to result in an error no larger than ±1%. However, and more importantly,
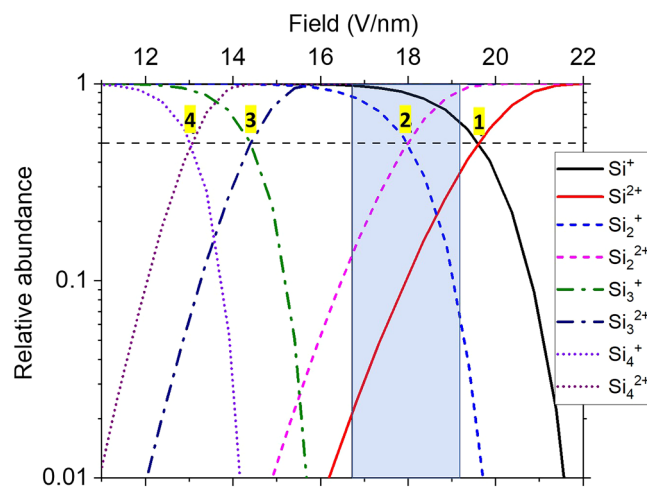
FIG. 1. PFI curves of Si and its clusters computed with an effective nuclear potential given by $Z = n + 1 + 4.5/z_0$, a principal quantum number $m_q = 3$, and a surface work function $\phi = 4.9$ eV. Note that the blue region indicates the range of electric field within which the experimental data lie. The yellow labels 1, 2, 3, and 4 indicate the F^{50} for Si, Si$_2$, Si$_3$, and Si$_4$ respectively.
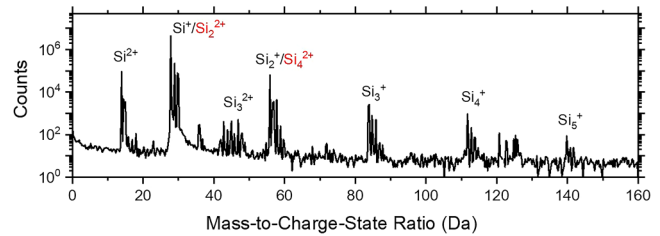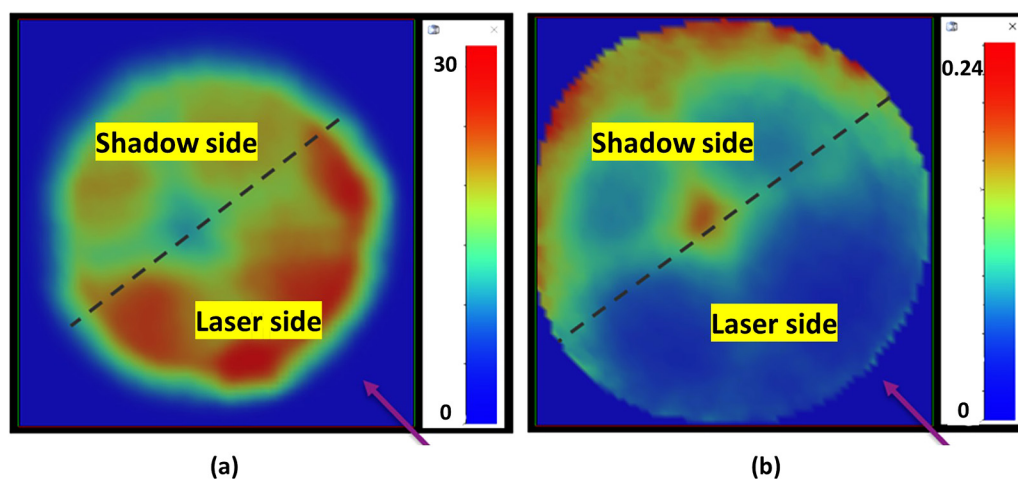
FIG. 3. An example of division of the dataset into two regions for data analysis. (a) 2D density plot of all ions. (b) 2D concentration plot of the Si^{2+} CSR [i.e., $Si^{2+}/(Si^{2+} + Si^{+})$] at an LPE of 110 pJ and detection rate of 0.5%. The laser direction is indicated by the violet arrow. Note that these plots are only representative of low to moderate LPE conditions. The Si-CSR distribution at high LPE values is anomalous, and two examples of this are given in the supplementary material. These data points were excluded from our PFI analysis.

the translation of these Si-CSRs into accurate electric field values is also subject to uncertainty. This is because the Kingham curve of monoatomic Si has not been experimentally validated thus far. Moreover, since there is no direct way to determine the electric field at the specimen apex during an APT experiment, any experimental verification of the Si Kingham curve would only be as accurate as the electric field calibration method used. Thus, the horizontal error bars will most certainly be much larger. As one would expect, this will also have serious implications for this work, and this will be discussed in Sec. IV B.

IV. DISCUSSION

A. Comparison of the experimental data with the model predictions

The experimental and theoretical F^{50} values and the second VIE values calculated by DFT are summarized in Table II. Both the experimental data and the theory indicate that the PFI of Si_2, Si_3, and Si_4 clusters occurs at a lower electric field compared to Si (re: F^{50} values). However, if we examine the experimental data from Figs. 4(a)–4(c) (solid symbols) and compare these, we find that the variation of F^{50} with cluster size does not agree with the model predictions.

To explain the poor fit quality, we assessed the potential impact of the model parameters on the quality of the fit. There are two parameters that require careful examination in the context of clusters, namely, the empirical expression used for the effective nuclear potential, Z, and the ionization energy. Additionally, two other model parameters, i.e., the principal quantum number (through the expression for the electron vibration frequency) and the work function, will influence the fit too. However, the sensitivity of the model to these last two quantities is extremely low, and it would require unreasonably large changes to these parameters to

match the data (details in the supplementary material). Thus, in this work, we will limit the discussion to the influence of Z and the ionization energy on the quality of the fit.

(1) Effective nuclear potential seen by the tunneling electron: The Kingham model was a single parameter fit applied to the Rh experimental data. The fitting parameter, Z, is the effective hydrogenic[19] nuclear potential as seen by the tunneling electron and is given by the empirical relation

$$Z = n + 1 + 4.5/z_0, \qquad (2)$$

where z_0 is the distance of the ion from the model surface and n is its initial charge-state. This potential will be a superposition of the electric potential due to the applied electric field and the ionic potential of field-evaporating ion. Thus, Z will essentially

TABLE II. The experimental and theoretical F^{50} values from Figs. 5 and 2, respectively. The second VIE computed using DFT (from Table 1) are displayed here to allow a correlation with the F^{50} values. The experimental F^{50} value for Si is taken to be equal to the theoretical value.

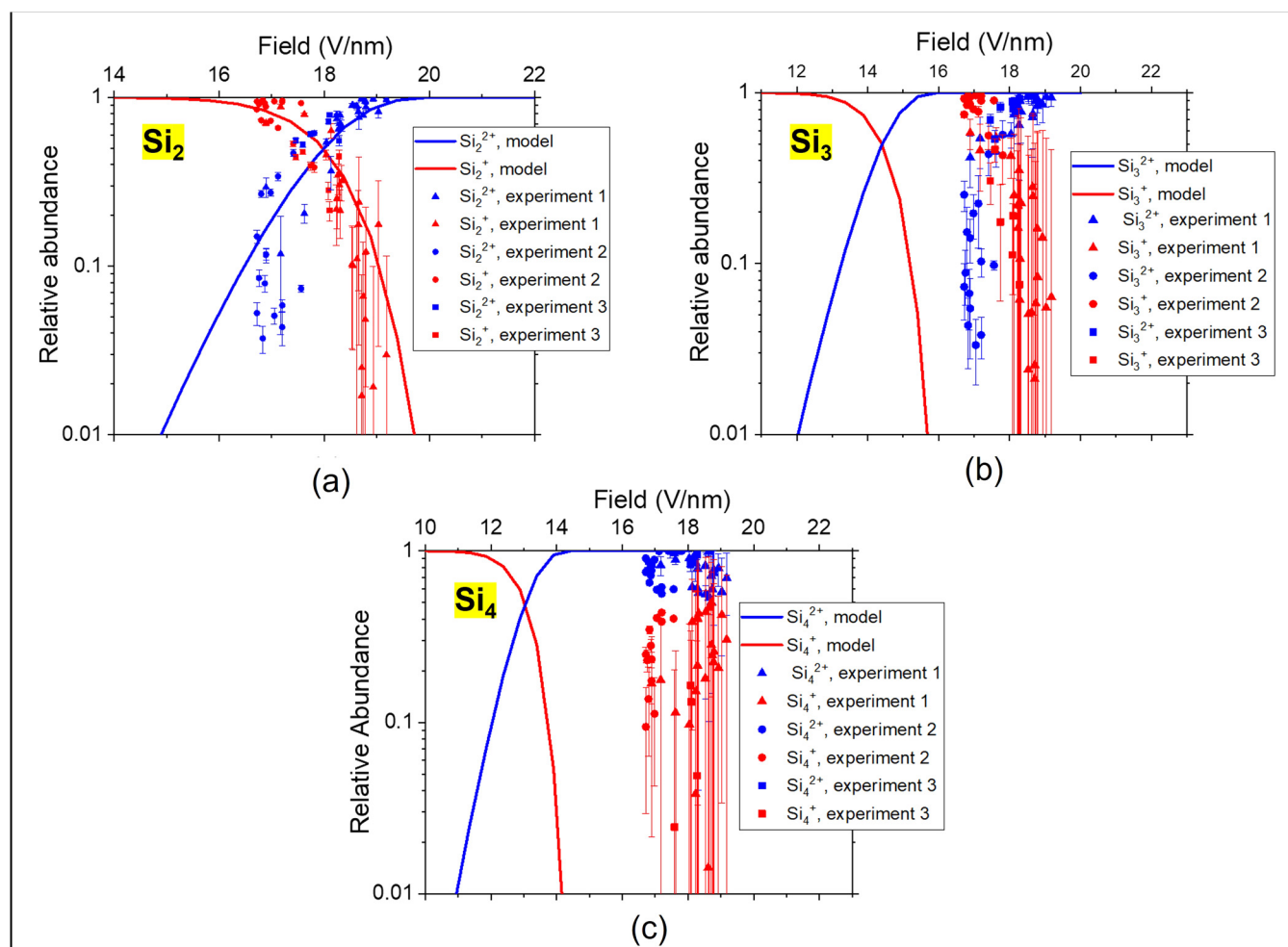| Species	F^{50} experimental (V/nm)	F^{50} theoretical (V/nm)	Second VIE (eV)
Si (used as the reference)	19.6	19.6	16.4
Si_2	17.7	18.0	15.8
Si_3	17.7	14.4	14.4
Si_4	<17.0	13.0	13.9

FIG. 4. Scatterplot of the experimental PFI data for (a) Si_2, (b) Si_3, and (c) Si_4. Vertical error bars on experimental data points indicate the 2σ error due to counting statistics. The solid lines in each figure correspond to the theoretical PFI curve computed using the VIEs calculated by DFT (Table I).

be a function of the final ionic charge-state $(n + 1)$ as well as the distance z_0. For a more detailed explanation on the choice of the above fitting function and its dependence on z_0, the reader is referred to Ref. 19. In keeping with Kingham's work, we used a similar function. However, due to the greater screening of the nuclear charge by the electrons in a molecule compared to an atom, it is possible that the effective nuclear charge seen by an electron that is tunneling out from a molecular ion will be lower than what is seen by an electron tunneling from a monoatomic ion. In accordance with this, decreasing the parameter Z has the effect of shifting the PFI curves toward the right, i.e., toward higher electric field, thus resulting in an improved fit to the experimental data. Since the model is a good fit to the Si_2 experimental data [Fig. 4(a)], this suggests that the original empirical function for Z (E2) is still an acceptable approximation for Si_2. However, for the larger clusters, it is possible that E2

overestimates Z. To improve the quality of the fit for Si_3 and Si_4, the coefficients of this polynomial were varied such that the theoretical and experimental F^{50} values agreed. A reasonably close fit to the experimental data was obtained by using the empirical expressions $Z' = n + 0.55 + 1/z_0$ for Si_3 and $Z' = n + 0.28 + 1/z_0$ for Si_4 (Fig. 5).

(2) **Cluster ionization energy:** For any given electric field, the PFI probability is extremely sensitive to the ionization energy [represented by the symbol "I" in E(S35) in the supplementary material]. Given that the second VIE of the Si clusters decreases with increasing size, the model predicts that the F^{50} values should also decrease monotonously. However, our experimental results would indicate that Si_2 and Si_3 have approximately the same experimental F^{50} value ($\sim$17.7 V/nm). The accuracy of IEs computed by DFT depends on the approximations used. Thus, it is standard practice to benchmark the approximations (primarily,
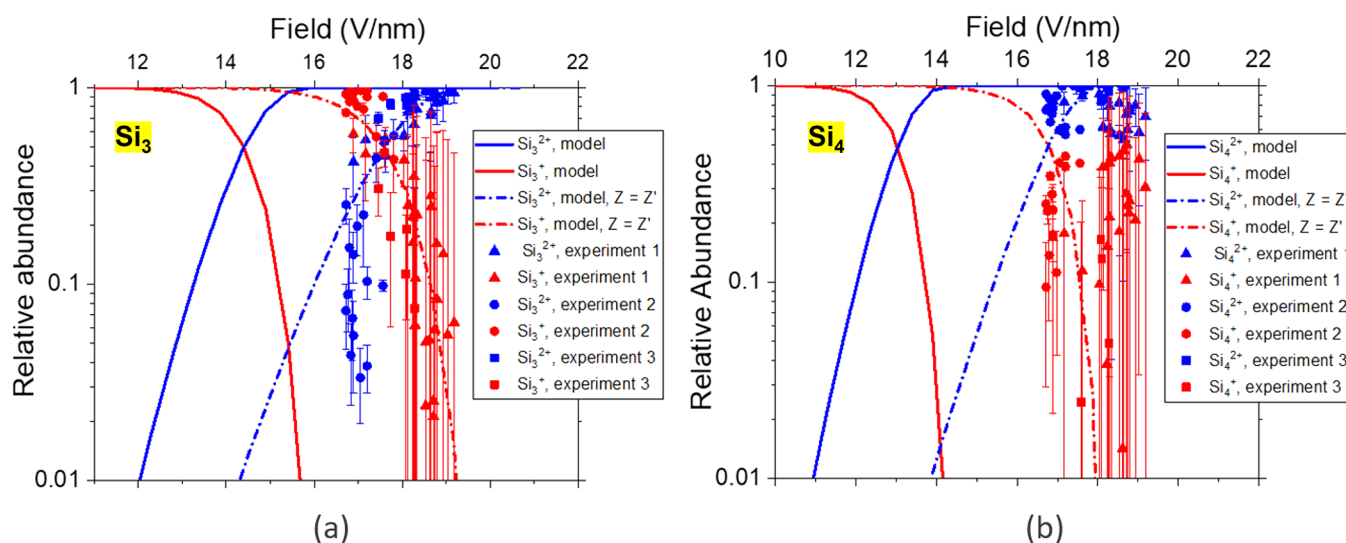
FIG. 5. Impact of decreasing Z on the PFI model (dashed lines) for (a) Si_3, using $Z' = n + 0.55 + 1/z_0$, and (b) Si_4, using $Z' = n + 0.28 + 1/z_0$. Also shown (solid lines) are the PFI curves computed using Z given by E2.

the energy functional) against experimental data of any other parameter that may be available for the same system. As was explained in Sec. II C, the approximations chosen for the Si cluster VIE calculations were benchmarked against experimental data of the first AIE of the Si clusters (see the supplementary material).[39] The intrinsic computational error on the VIE values is, therefore, not expected to be greater than ~0.2 eV.[41] However, an important effect that is not considered in the DFT calculations presented here is the impact of the electric field on the IEs. In an electric field, the molecular orbitals will become polarized, and the electrons will interact with the electric field. This has an impact on how the electrons interact with the ion core and leads to the electronic energy levels becoming more negative,[19] effectively increasing the IE of the molecule. The deviation of the model predictions (for Si_3 and Si_4) from the experimental data could potentially be explained by the effect of the electric field on the IE of these clusters. For these clusters and by varying the VIE values, a better agreement between the theory and experimental data is achieved with a ~9.8% and ~13% increase of the second VIE for Si_3 and Si_4, respectively [dashed lines, Figs. 6(a) and 6(b)]. This corresponds to an increase of the second VIE by 1.41 eV (Si_3) and 1.55 eV (Si_4). It is unclear whether this magnitude of electric field-induced IE shift is realistically possible and is a non-trivial question to answer. Although there are some recent literature studies about the impact of the electric field on the molecular orbitals in the context of APT using *ab initio* and molecular dynamics simulations,[42–44] to the best of the authors' knowledge, there are currently no reported studies on the quantitative impact of the electric field on the IEs of molecular ions. While it would be worthwhile to investigate this further, at this stage, we note that it is more practical to treat Z as the only fitting parameter while using electric field-free VIE values in the model, primarily because of the complexity involved in

computationally/experimentally estimating the shift of the clusters VIEs due to an electric field.

B. Resolving peak overlap for monoisotopic species using cluster PFI curves—Challenges and ways forward

To assess whether the above conclusions are transferrable to another system and can be used to resolve peak overlap between clusters of monoisotopic species, as proposed initially, we considered the PFI of As clusters in the APT of InGaAs. In general, for examining the applicability of this method to other molecular ions, which could be relatively unstable in an electric field, their in-flight dissociation will have to be considered during experimental data treatment. However, this is not expected to be a significant problem for As clusters.[17] The electric field dependence of the InGaAs composition determined by APT was investigated in detail in a previous study,[17] which revealed that the As content was underestimated for nearly all operating conditions. From the analysis, it was concluded that mass peak overlaps were the most important source of compositional inaccuracy. From that study, we chose an operational electric field regime (laser pulse energy = 0.1 pJ; In-CSR = 0.0056), where the As content determined by APT was 46.5 at. % (whereas its nominal value should be 50 at. %). The mass spectrum acquired at these conditions is shown in Fig. 7, with all the As cluster peaks indicated. The As_6^+ mass peak (450 Da) is absent and, thus, it is reasonable to assume that As_6^{2+} is not emitted. Moreover, As_5 is also absent and the As_5^{2+} peak has negligible counts, which further justifies this assumption. This means that there will be no interference with As_3^+ at 225 Da. The inset in Fig. 7 shows the number of ionic counts at each mass peak. Two of these peaks could potentially be impacted by overlap, namely, the peak at 150 Da, which could contain As_4^{2+} and As_2^+, and the peak at 75 Da, which could contain As_2^{2+} and As^+. In attempting to resolve
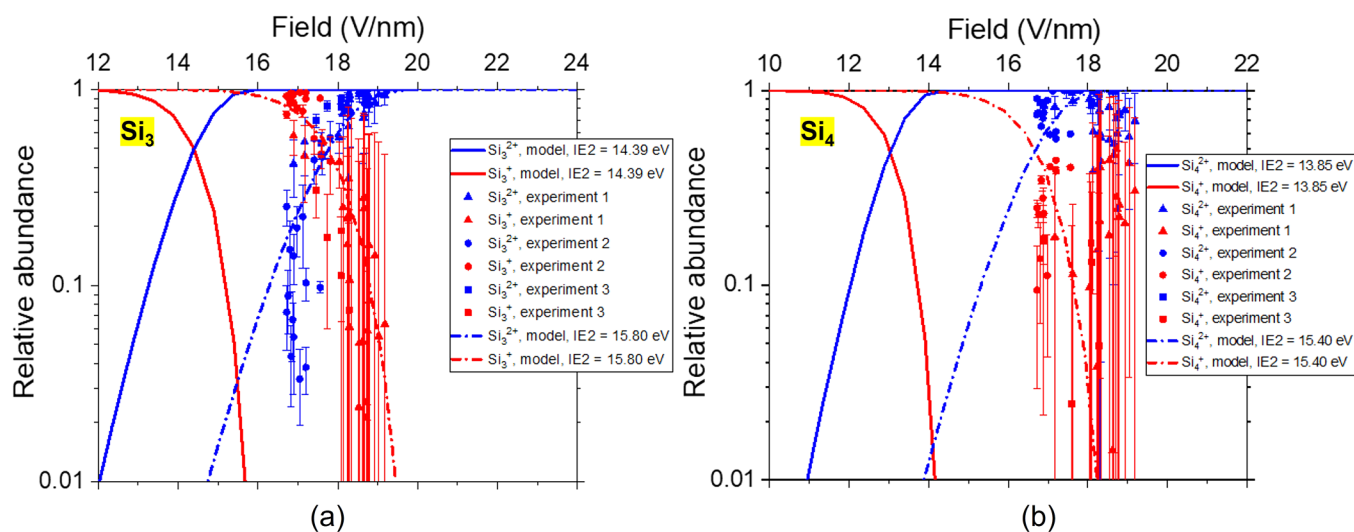
FIG. 6. Impact of varying the second VIE on the PFI model (dashed lines) for (a) Si_3 and (b) Si_4. Also shown (solid lines) are the PFI curves computed using the electric field-free VIE values (Table I). In (a), the solid lines were calculated using an IE2 = 14.39 eV, whereas the dashed lines were calculated using an IE2 = 15.80 eV to obtain a better fit to the data. Similarly, in (b), the solid lines were calculated using an IE2 = 13.85 eV, whereas the dashed lines were calculated using an IE2 of 15.40 eV to obtain a better fit to the data.
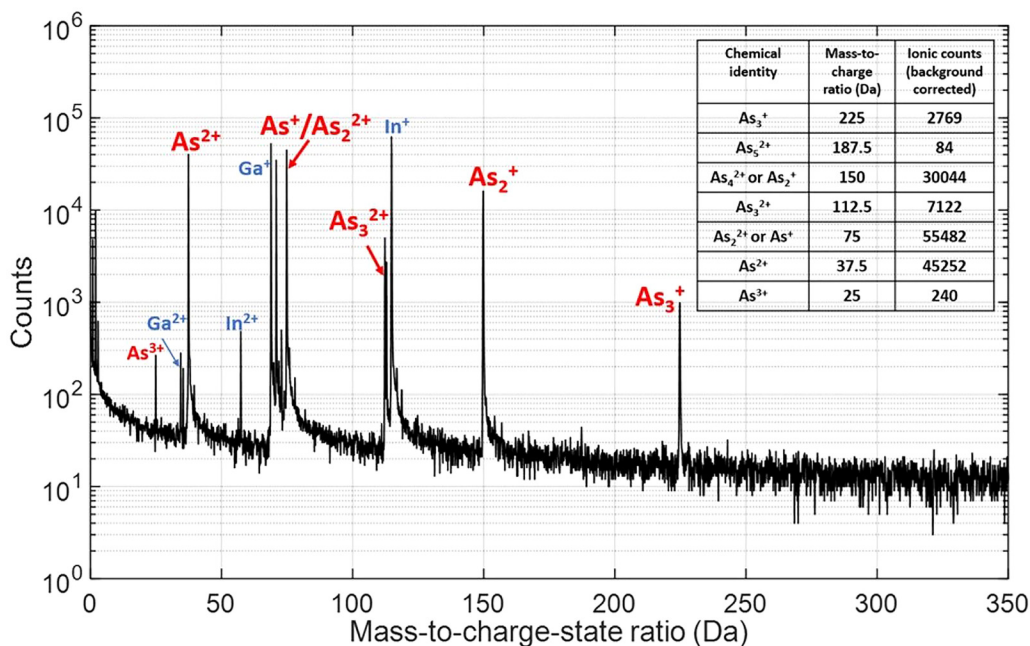
FIG. 7. The mass spectrum of InGaAs acquired on the Cameca LEAP 5000XR at a laser pulse energy of 0.1 pJ and an In-CSR of 0.0056. The inset indicates the total number of ionic counts present in each peak corresponding to the As clusters.

these two overlaps using PFI theory, four main inconsistencies in the results were found, which indicated that further refinements to this approach will be required before it can be used as a standalone technique for resolving overlap. The procedure followed and the inconsistencies encountered therein are described in detail below.

1. The In-CSR together with the In Kingham curve was first used to calibrate the experimental data against the electric field. For this case, the electric field was determined to be 21.3 V/nm.
2. The theoretical PFI curves of As_2, As_3, and As_4 were then computed using the corresponding expression for Z' that best matched the Si_2, Si_3, and Si_4 experimental data, respectively. The As cluster VIE values used for this calculation are reported in Ref. 17. These three As cluster PFI curves along with the monoatomic As PFI

curve are indicated in Fig. 8 by the solid lines. From these curves, at an electric field of 21.3 V/nm, we obtain the following:
(a) $As_2^{2+}/(As_2^{2+} + As^+) = 0.0143$,
(b) $As_2^{2+}/(As_2^{2+} + As_2^+) = 1.0000$,
(c) $As_3^{2+}/(As_3^{2+} + As_3^+) = 0.9468$, and
(d) $As_4^{2+}/(As_4^{2+} + As_4^+) = 1.0000$.

3. From 2(b), the counts of As_2^+ should be zero. This essentially means that any counts present at 150 Da should belong to As_4^{2+}. However, upon assigning all counts at 150 Da to As_4^{2+}, we obtain a revised As content of 53 at. %, which exceeds the nominal value and thus is an incorrect prediction.
4. Furthermore, since the As_3 and As_3^{2+} peaks in this case do not suffer from any overlaps, it is possible to compare the theoretical As_3 PFI curve with the experiment [Fig. 8(c), solid lines vs solid
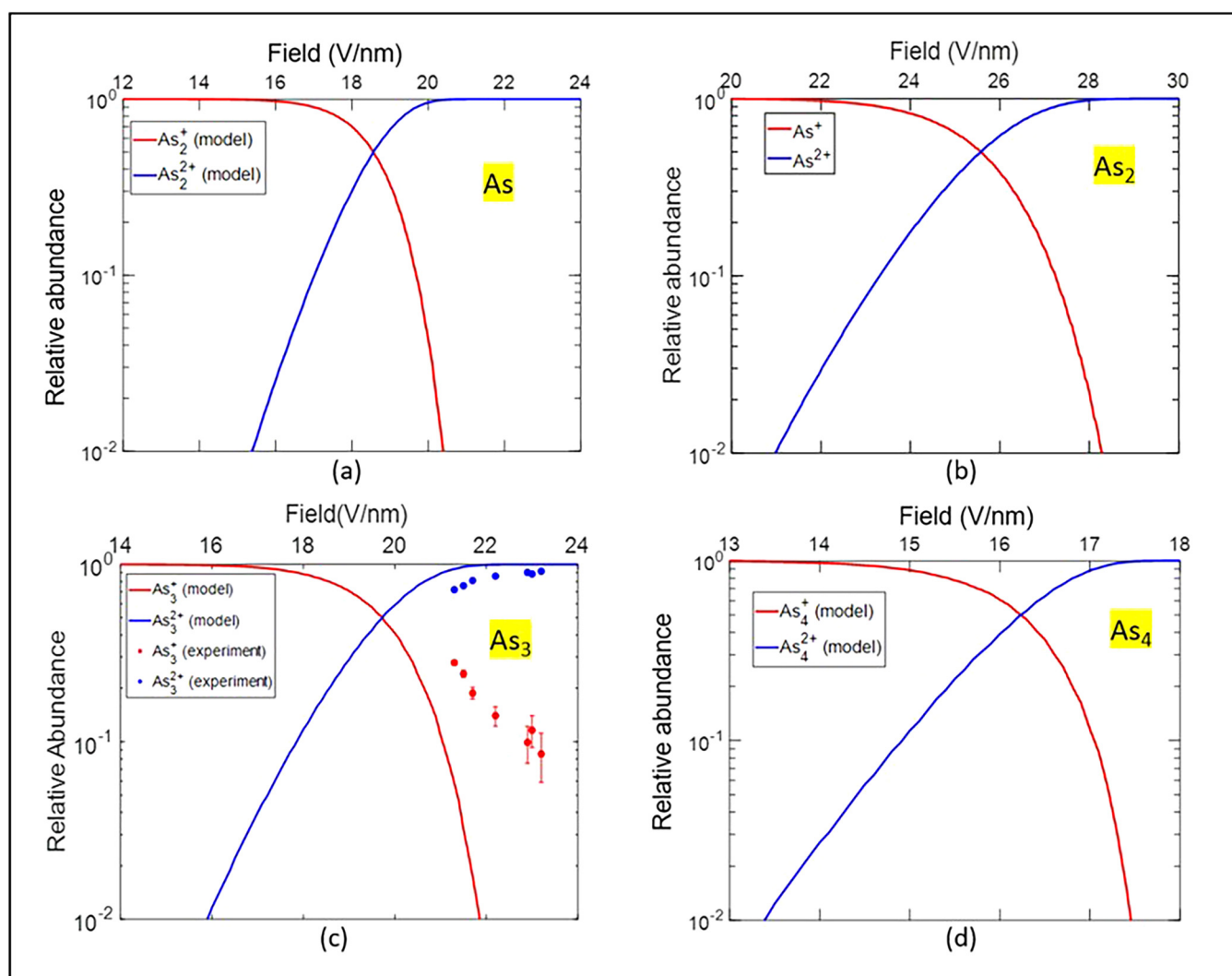

FIG. 8. Theoretical PFI curves (solid lines) of (a) As, (b) As_2, (c) As_3, and (d) As_4. Also indicated in (c) are the experimental As_3 data (solid symbols).

symbols]. Unfortunately, the agreement with the theoretical predictions is poor. Upon extrapolation, the experimental F^{50} value will most likely be slightly greater than the theoretical value of 19.7 V/nm.

5. At 75 Da, we have 55 482 background corrected counts, some of which are As_2^{2+} and the rest are As^+. Using 2(a) and the counts at 37.5 Da (As^{2+}), we can compute the fraction of counts that should be attributed to As^+. However, this leads to unrealistic results, i.e., the model's prediction of the As^+ counts exceeds the available counts in the 75 Da peak.

6. Additionally, the presence of As^{3+} at 25 Da in the mass spectrum (Fig. 7) is unexpected since it is inconsistent with the monoatomic As PFI curve [Fig. 8(a)] according to which As^{3+} should not be observed at an electric field of 21.3 V/nm.

There are two bottlenecks for achieving reliable results. First, the PFI model currently does not accurately represent the physical reality, especially for molecules. Since the Kingham model has been verified experimentally for very few elements and the approach proposed in this work relies on the assumption that this model would work equally well for all other elements, it leads to a huge uncertainty in the results. If this assumption were, in fact, true, then using any monoatomic CSR (and its PFI curve) to estimate the electric field and subsequently estimate the overlap between clusters at that electric field would yield accurate results. Since the validity of this assumption cannot be established currently, any electric field determination method based on the Kingham model will be rendered arbitrary. This essentially means that the Kingham model itself would benefit from further refinement, i.e., PFI theory for both molecular and monoatomic ions deserve more attention. Based on the criticism of Kingham's model in later work,[45] it is worth examining alternative approaches to calculate the electron tunneling rate constant. Particularly, for molecules, a more complex approach may be required. Moreover, the decay of the electric field strength as a function of the distance from the emitter surface and its impact on the PFI probability also need to be accounted for. Most importantly, there is a need for standardizing the PFI model/equations used and its calculation across the APT community.

Second, the development of a more refined PFI model would necessarily require experimental data against which the model can be validated. To obtain such (reliable) experimental data, an accurate electric field determination/calibration procedure would be required, and this presents an additional challenge. As discussed in Ref. 46, there are currently no tested methods to experimentally measure (directly or indirectly) the average electric field at the apex of the APT specimen. This is because the radius of the specimen at any given instant during data acquisition is unknown. Upcoming *in situ* techniques that would potentially be able to probe this information involve the incorporation of an atom probe within a transmission electron microscope, which in itself is a massive undertaking and still in an early developmental stage.[47]

V. CONCLUSIONS

This work was an experimental investigation of the PFI behavior of molecular/cluster ions in APT. We have shown that the charge-state variation of Si clusters Si_2 and Si_3 as a function of the electric field is qualitatively consistent with the predictions of PFI theory, i.e., the fraction of doubly charged species increases with the electric field. However, the variation of the F^{50} value as a function of the cluster size showed a poor agreement between the experimental data and theoretical predictions. The main reason for the quantitative disagreement is the simplicity of assumptions made in the model parameters when extending the Kingham model, which was originally developed for monoatomic ions, to molecules. Based on experimental data of the Si clusters, the model parameters could be re-calibrated to yield an improved fit. However, upon applying this revised model to resolve peak overlap between As clusters, several inaccuracies were found, thus indicating that the PFI theory (for both monoatomic and molecular species) and electric field calibration methods need further development. If a more detailed model can be developed in the future, then it would be worth re-evaluating the transferability of the proposed concept and its feasibility for resolving peak overlap.

SUPPLEMENTARY MATERIAL

The supplementary material of this manuscript contains a detailed description of the Kingham PFI model, our calculations of the PFI curves, and the details of the DFT calculations of the Si cluster ionization energies.

AUTHOR DECLARATIONS

Conflict of Interest

The authors have no conflicts to disclose.

Author Contributions

Ramya Cuduvally: Conceptualization (lead); Formal analysis (lead); Investigation (lead); Methodology (lead); Software (lead); Validation (lead); Visualization (lead); Writing – original draft (lead); Writing – review & editing (lead). **Richard J. H. Morris:** Conceptualization (supporting); Supervision (supporting); Writing – review & editing (supporting). **Giel Oosterbos:** Software (supporting); Validation (supporting); Writing – review & editing (supporting). **Piero Ferrari:** Software (supporting); Supervision (supporting); Writing – review & editing (supporting). **Claudia Fleischmann:** Writing – review & editing (supporting). **Richard G. Forbes:** Conceptualization (supporting); Supervision (supporting); Writing – review & editing (supporting). **Wilfried Vandervorst:** Conceptualization (supporting); Funding acquisition (lead); Project administration (lead); Supervision (lead); Writing – review & editing (supporting).

DATA AVAILABILITY

The datasets and code used in the current study are available from the corresponding author upon reasonable request.

REFERENCES

[1]B. Deconihout, A. Bostel, P. Bas, S. Chambreland, L. Letellier, F. Danoix, and D. Blavette, "Investigation of some selected metallurgical problems with the tomographic atom probe," Appl. Surf. Sci. **76–77**, 145–154 (1994).

[2]H. Takamizawa, Y. Shimizu, K. Inoue, T. Toyama, N. Okada, M. Kato, H. Uchida, F. Yano, A. Nishida, T. Mogami, and Y. Nagai, "Origin of characteristic variability in metal-oxide-semiconductor field-effect transistors revealed by three-dimensional atom imaging," Appl. Phys. Lett. **99**, 133502 (2011).

[3]L. J. Lauhon, P. Adusumilli, P. Ronsheim, P. L. Flaitz, and D. Lawrence, "Atom-probe tomography of semiconductor materials and device structures," MRS Bull. **34**, 738–743 (2009).

[4]A. K. Kambham, A. Kumar, A. Florakis, and W. Vandervorst, "Three-dimensional doping and diffusion in nano scaled devices as studied by atom probe tomography," Nanotechnology **24**, 275705 (2013).

[5]T. F. Kelly, D. J. Larson, K. Thompson, R. L. Alvis, J. H. Bunton, J. D. Olson, and B. P. Gorman, "Atom probe tomography of electronic materials," Annu. Rev. Mater. Res. **37**, 681–727 (2007).

[6]D. W. Saxey, D. E. Moser, S. Piazolo, S. M. Reddy, and J. W. Valley, "Atomic worlds: Current state and future of atom probe tomography in geoscience," Scr. Mater. **148**, 115–121 (2018).

[7]L. M. Gordon, L. Tran, and D. Joester, "Atom probe tomography of apatites and bone-type mineralized tissues," ACS Nano. **6**, 10667–10675 (2012).

[8]T. F. Kelly, "Kinetic-energy discrimination for atom probe tomography," Microsc. Microanal. **17**, 1–14 (2011).

[9]C. Bacchi, G. Da Costa, E. Cadel, F. Cuvilly, J. Houard, C. Vaudolon, A. Normand, and F. Vurpillot, "Development of an energy-sensitive detector for the atom probe tomography," Microsc. Microanal. **28**, 1076–1091 (2022).

[10]D. J. Larson, T. J. Prosa, R. M. Ulfig, B. P. Geiser, and T. F. Kelly, *Local Electrode Atom Probe Tomography* (Springer, New York, 2013).

[11]E. Simoen, P.-C. B. Hsu, H. Yu, H. Wang, M. Zhao, K. Takakura, V. Putcha, U. Peralagu, B. Parvais, N. Waldron, and N. Collaert, "Materials and defect aspects of III-V and III-N devices for high-speed analog/RF applications," in *2020 IEEE 15th International Conference on Solid-State and Integrated Circuit Technology (ICSICT)* (IEEE, 2020), pp. 1–4.

[12]O. Marshall, M. Hsu, Z. Wang, B. Kunert, C. Koos, and D. V. Thourhout, "Heterogeneous integration on silicon photonics," Proc. IEEE **106**, 2258–2269 (2018).

[13]B. Liu, D. Chen, H. Lu, T. Tao, Z. Zhuang, Z. Shao, W. Xu, H. Ge, T. Zhi, F. Ren, J. Ye, Z. Xie, and R. Zhang, "Hybrid light emitters and UV solar-blind avalanche photodiodes based on III-nitride semiconductors," Adv. Mater. **32**, 1904354 (2019).

[14]H. Amano, Y. Baines, E. Beam, M. Borga, T. Bouchet, P. R. Chalker, M. Charles, K. J. Chen, N. Chowdhury, R. Chu, C. De Santi, M. M. De Souza, S. Decoutere, L. Di Cioccio, B. Eckardt, T. Egawa, P. Fay, J. J. Freedsman, L. Guido, O. Häberlen, G. Haynes, T. Heckel, D. Hemakumara, P. Houston, J. Hu, M. Hua, Q. Huang, A. Huang, S. Jiang, H. Kawai, D. Kinzer, M. Kuball, A. Kumar, K. B. Lee, X. Li, D. Marcon, M. März, R. McCarthy, G. Meneghesso, M. Meneghini, E. Morvan, A. Nakajima, E. M. S. Narayanan, S. Oliver, T. Palacios, D. Piedra, M. Plissonnier, R. Reddy, M. Sun, I. Thayne, A. Torres, N. Trivellin, V. Unni, M. J. Uren, M. Van Hove, D. J. Wallis, J. Wang, J. Xie, S. Yagi, S. Yang, C. Youtsey, R. Yu, E. Zanoni, S. Zeltner, and Y. Zhang, "The 2018 GaN power electronics roadmap," J. Phys. D: Appl. Phys. **51**, 163001 (2018).

[15]C. Schwinge, K. Kühnel, J. Emara, L. Roy, K. Biedermann, W. Weinreich, S. Kolodinski, M. Wiatr, G. Gerlach, and M. Wagner-Reetz, "Optimization of LPCVD phosphorous-doped SiGe thin films for CMOS-compatible thermoelectric applications," Appl. Phys. Lett. **120**, 031903 (2022).

[16]Y. Ohno, T. Yokoi, Y. Shimizu, J. Ren, K. Inoue, Y. Nagai, K. Kutsukake, K. Fujiwara, A. Nakamura, K. Matsunaga, and H. Yoshida, "Segregation mechanism of arsenic dopants at grain boundaries in silicon," Sci. Technol. Adv. Mater. Methods **1**, 169–180 (2021).

[17]R. Cuduvally, R. J. H. Morris, P. Ferrari, J. Bogdanowicz, C. Fleischmann, D. Melkonyan, and W. Vandervorst, "Potential sources of compositional inaccuracy in the atom probe tomography of $In_xGa_{1-x}As$," Ultramicroscopy **210**, 112918 (2020).

[18]E. Di Russo, I. Blum, I. Rivalta, J. Houard, G. Da Costa, F. Vurpillot, D. Blavette, and L. Rigutti, "Detecting dissociation dynamics of phosphorus molecular ions by atom probe tomography," J. Phys. Chem. A **124**, 10977–10988 (2020).

[19]D. R. Kingham, "The post-ionization of field evaporated ions: A theoretical explanation of multiple charge states," Surf. Sci. **116**, 273–301 (1982).

[20]T. T. Tsong, "Pulsed-laser-stimulated field ion emission from metal and semiconductor surfaces: A time-of-flight study of the formation of atomic, molecular, and cluster ions," Phys. Rev. B **30**, 4946–4961 (1984).

[21]N. Ernst, "Experimental investigation on field evaporation of singly and doubly charged rhodium," Surf. Sci. **87**, 469–482 (1979).

[22]N. Ernst and Th. Jentsch, "Post-field ionization of singly charged rhodium: An experimental and theoretical study," Phys. Rev. B **24**, 6234–6241 (1981).

[23]R. Haydock and D. R. Kingham, "Post-Ionization of field-evaporated ions," Phys. Rev. Lett. **44**, 1520–1523 (1980).

[24]R. Haydock and D. R. Kingham, "Some predictions of a theory of post-ionization of field-evaporated ions," Surf. Sci. **104**, L194–L198 (1981).

[25]R. Haydock and D. R. Kingham, "Field ionization theory: A new, analytic, formalism," Surf. Sci. **103**, 239–247 (1981).

[26]G. L. Kellogg, "Measurement of the charge state distribution of field evaporated ions: Evidence for post-ionization," Surf. Sci. **120**, 319–333 (1982).

[27]E. W. Müller and R. D. Young, "Determination of field strength for field evaporation and ionization in the field Ion microscope," J. Appl. Phys. **32**, 2425–2428 (1961).

[28]D. K. Schreiber, A. N. Chiaramonti, L. M. Gordon, and K. Kruska, "Applicability of post-ionization theory to laser-assisted field evaporation of magnetite," Appl. Phys. Lett. **105**, 244106 (2014).

[29]B. Gault, D. W. Saxey, M. W. Ashton, S. B. Sinnott, A. N. Chiaramonti, M. P. Moody, and D. K. Schreiber, "Behavior of molecules and molecular ions near a field emitter," New J. Phys. **18**, 033031 (2016).

[30]Y. H. Chang, I. Mouton, L. Stephenson, M. Ashton, G. K. Zhang, A. Szczpaniak, W. J. Lu, D. Ponge, D. Raabe, and B. Gault, "Quantification of solute deuterium in titanium deuteride by atom probe tomography with both laser pulsing and high-voltage pulsing: Influence of the surface electric field," New J. Phys. **21**, 053025 (2019).

[31]A. Kumar, "Qualitative and quantitative analysis of compound semiconductors using atom probe tomography," Ph.D. thesis (KU Leuven, 2016), see https://lirias.kuleuven.be/1762255?limo=0.

[32]T. Ono and K. Hirose, "First-principles study on field evaporation for silicon atom on Si(001) surface," J. Appl. Phys. **95**, 1568–1571 (2004).

[33]G. Oosterbos, "Post-ionization of silicon clusters in atom probe microscopy: A theoretical and experimental comparison," Master's thesis (KU Leuven, 2019).

[34]D. A. McQuarrie and J. D. Simon, *Physical Chemistry: A Molecular Approach* (University science books, Sausalito, CA, 1997), Vol. 1.

[35]K. Thompson, D. J. Larson, and R. M. Ulfig, "Pre-sharpened and flat-top microtip coupons: A quantitative comparison for atom-probe analysis studies," Microsc. Microanal. **11**, 882 (2005).

[36]F. Neese, "The ORCA program system," WIREs Comput. Mol. Sci. **2**, 73–78 (2012).

[37]Y.-S. Lin, G.-D. Li, S.-P. Mao, and J.-D. Chai, "Long-range corrected hybrid density functionals with improved dispersion corrections," J. Chem. Theory Comput. **9**, 263–272 (2013).

[38]F. Weigend and R. Ahlrichs, "Balanced basis sets of split valence, triple zeta valence and quadruple zeta valence quality for H to Rn: Design and assessment of accuracy," Phys. Chem. Chem. Phys. **7**, 3297–3305 (2005).

[39]O. Kostko, S. R. Leone, M. A. Duncan, and M. Ahmed, "Determination of ionization energies of small silicon clusters with vacuum ultraviolet radiation," J. Phys. Chem. A **114**, 3176–3181 (2010).

[40]B. Gault, M. P. Moody, J. M. Cairney, and S. P. Ringer, *Atom Probe Microscopy* (Springer, New York, 2012).

[41]K. Capelle, "A bird's-eye view of density-functional theory," Braz. J. Phys. **36**, 1318–1343 (2006).

[42]D. Zanuttini, F. Vurpillot, J. Douady, E. Jacquet, P.-M. Anglade, and B. Gervais, "Dissociation of GaN^{2+} and AlN^{2+} in APT: Electronic structure and stability in strong DC field," J. Chem. Phys. **149**, 134310 (2018).

[43]Z. Peng, D. Zanuttini, B. Gervais, E. Jacquet, I. Blum, P. P. Choi, D. Raabe, F. Vurpillot, and B. Gault, "Unraveling the metastability of C_n^{2+} (n = 2–4) clusters," J. Phys. Chem. Lett. **10**, 581–588 (2019).

[44]D. Zanuttini, I. Blum, L. Rigutti, F. Vurpillot, J. Douady, E. Jacquet, P.-M. Anglade, and B. Gervais, "Electronic structure and stability of the SiO^{2+} dications produced in tomographic atom probe experiments," J. Chem. Phys. **147**, 164301 (2017).

[45]S. C. Lam and R. J. Needs, "Calculations of ionization rate-constants for the field-ion microscope," Surf. Sci. Lett. **277**, 359 (1992).

[46]R. G. Forbes, "Field calibration issues," in *Physics of Solid Surfaces* (Springer, 2018), pp. 658–662.

[47]T. Kelly, R. Dunin-Borkowski, and J. Meyer, "Project Tomo: Toward atomic-scale analytical tomography," Microsc. Microanal. **26**, 2618–2621 (2020).